JMEPEG (2013) 22:1593–1600
DOI: 10.1007/s11665-013-0471-9

1059-9495/$19.00

# Elastic Properties of UHMWPE-SWCNT Nanocomposites' Fiber: An Experimental, Theoretic, and Molecular Dynamics Evaluation

*Mujibur R. Khan, Hassan Mahfuz, Ashfaq Adnan, Ishraq Shabib, and Theodora Leventouri*

*(Submitted October 10, 2012; in revised form December 2, 2012; published online January 24, 2013)*

**Ultrahigh molecular weight polyethylene (PE) filaments were reinforced with 2 wt.% of single-walled carbon nanotubes (SWCNTs). The solution spinning method was used to produce both neat and reinforced PE filaments. Tensile tests and strain hardening through repeated loading-unloading cycles of the filaments revealed a spectacular contribution of the SWCNTs in enhancing the elastic properties, e.g., strength and modulus. The theoretic strength and modulus of the reinforced PE were predicted using the shear lag model and micromechanics-based model, respectively, and verifying with experimental results. It was observed that the predicted strength and modulus were comparable only with those obtained after strain hardening. In the next step, a molecular dynamic simulation was conducted by simulating a unit cell containing a SWCNT surrounded by PE matrix subjected to uniaxial tensile strain. The strength and modulus of the simulated structure showed an agreement, to certain extent, with experimental observations of strain-hardened nanocomposites.**

**Keywords** molecular model, shear lag model, solution spinning, strain hardening, SWCNT, UHMWPE

## 1. Introduction

The unique structure of CNTs provides a superior reinforcing effect to the polymer (Ref 1-3). In order to utilize the extraordinary strength and stiffness of carbon nanotubes, several researchers have attempted to align CNTs along preferred directions in the bulk materials (Ref 4-10). Almost all of these attempts were made with the infusion of single or multiwalled CNTs or vapor-grown carbon nanofibers (CNF) into thermoplastic polymers. Infusion was carried out either through a liquid route using sonication or a dry route followed by melt mixing in an extruder. Alignment of CNTs or CNFs in the composite was enforced by extrusion or the spinning technique. The resulting composites, either in consolidated or filament form, have demonstrated improved mechanical and thermal properties. These properties of nanotube-polymer composites are strongly influenced by the dispersion, aspect ratio, and alignment of the nanotubes within the matrix. As these factors are independent, control experiments were challenging. For example, CNTs have substantial van der Waals attractions between them and tend to agglomerate. Moreover, when CNTs agglomerate or form bundles, their aspect ratio becomes significantly low and the mechanical properties become inferior. Therefore, uniformly dispersed nanotubes and their alignment within the polymer matrix are critical for improved properties.

It has also been revealed that the ability of the polymer fibrils to undergo molecular orientation through strain hardening can greatly enhance the strength and stability of the craze structure (Ref 11, 12). Strain hardening in polymers is thought to be primarily due to the effects of orientation. Since the anisotropic nature of the chemical bonding in ultrahigh molecular weight polyethylene (UHMWPE) can cause a highly oriented polymer, strength and stiffness are expected to increase through strain hardening sequences. Moreover, inclusion of CNTs can further increase the polymers' hardening ability (Ref 13). Increased strain hardening effects were also observed at large strains in polyethylene (PE) when reinforced with MWCNTs. It was reported that MWCNTs acted as tie molecules to induce strain hardening effects (Ref 14).

Nevertheless, prediction of the resulting properties of the composites is a very complex problem due to the many variables that play definite roles upon the mechanical behavior of these materials. In many cases, upper and lower bounds of modulus were studied using micromechanics, taking into consideration the volume fraction of the filler particles (Ref 15). The ultimate strength prediction was more rigorous due to the fact that interfacial adhesion between the matrix and the filler is of primary importance for load transfer and it is a difficult parameter to measure. The stress transfer problem for traditional fiber-reinforced composites has been extensively studied (Ref 16).The shear-lag model originally proposed by Cox (Ref 17) provides a good estimation of the stress in the fiber transferred in the matrix through the interface. Given the

**Mujibur R. Khan**, Department of Mechanical Engineering, Georgia Southern University, Statesboro, GA 30460; **Hassan Mahfuz**, Ocean & Mechanical Engineering Department, Florida Atlantic University, Boca Raton, FL 33431; **Ashfaq Adnan**, Department of Mechanical Engineering, University of Texas at Arlington, Arlington, TX 76019; **Ishraq Shabib**, Department of Mechanical Engineering, University of Texas at El Paso, El Paso, TX 79968; and **Theodora Leventouri**, Physics Department, Florida Atlantic University, Boca Raton, FL 33431. Contact e-mail: mkhan@georgiasouthern.edu.

fact that CNTs are fiber-like structures and a strong interaction exists between the nanotubes and the polymer matrix, this continuum-based approach has been used to predict the strength of the composites. The shear-lag analysis was developed in the context of linear elasticity and the resulting models were derived in closed form. However, the ambiguities come from the fact that nanomaterials are greatly influenced by the local motions of a discrete set of atoms and by the dominant presence of intermolecular and surface forces. Molecular dynamics (MD) simulation is a tool for the molecular-level study of the influence of nanoparticles on the structure and dynamics of polymers to predict the elastic properties of the composites (Ref 18). The nature of the interfacial bonding energy comes from the electrostatic and Van der Waals forces in the molecular system. From an atomic modeling viewpoint, the CNT-PE system is the most straightforward system to study because only two types of atoms, that is carbon and hydrogen, are involved, and the bonding types are well defined. Frankland et al. (Ref 19, 20) used two force field expressions: one which assumed a "united-atom" approximation and another which explicitly included hydrogen atoms to model PE matrices within which single-shelled (10, 10) CNTs were embedded. Similar modeling results were reported by Griebel and Hamaekers (Ref 21), where stress-strain relations were calculated using applied external stresses.

In spite of the evolution in the theoretic prediction methods of the elastic properties of the CNT-polymer composites, significant discrepancies are still observed in the experimental and the predicted property values. In most of the cases, the composite properties from the tensile tests were far less than the predicted upper limit. The possible reason can be that the resulting micro- and nanostructures from the material processing technique may not be in accordance with the theoretic idealization. However, systematic processing technique can result in the properties which are close to the theoretic prediction limit. This study aims to evaluate the elastic properties of UHMWPE-SWCNT composites in the form of filaments before and after strain hardening. The experimentally evaluated properties were compared with the theoretically predicted values from continuum-based micromechanics and MD simulation.

## 2. Experimental

### 2.1 Filament Manufacturing

Commercial-grade UHMWPE powder, paraffin oil, and anti-oxidant 2,6-di-*t*-butyl,4-methylcresol and single-walled carbon nanotubes (SWCNTs) were procured from Sigma Aldrich Co. (6000 North Teutonia Avenue Milwaukee, Wisconsin). As-received nanotubes were approximately 1-2 nm in diameter and 2-5 μm in length. Filaments were fabricated using a Laboratory Mixing Extruder (LME). The extrusion apparatus included a hexane bath, an oven, and a filament take-up system. A VCX 500 ultrasonic processor and a homogenizer (VDI 25) were used for dispersion of nanotubes. In the synthesis of neat filaments, SWCNTs at 2 wt.% of polymer were first dispersed into paraffin oil using sonication (60 Hz and at 45% intensity) for an hour. UHMWPE at 4.9 wt.% and the anti-oxidant at 0.5 wt.% were then mixed with 94.5 wt.% of paraffin oil using the homogenizer. The anti-oxidant was used to prevent oxidative degradation of the PE. The admixture was fed into a single screw extruder for melt mixing at around 150 °C and extruded through an orifice. The extrudate was rinsed via a hexane bath, stabilized through a heater (100 °C), and then drawn into a filament winder with controlled stretching. Hexane extracts the solvent paraffin oil from the gel filament. Cut filament strands were again heated in a separate oven to 60-70 °C for a prolonged period of time (~48 h) in order to remove residual solvent from the filament. The control samples were produced following the identical process, except for the sonication of SWCNT. The diameters of the post-fabricated filaments were then measured using a Scanning Electron Microscope.

It is to be mentioned here that we came up with the 2% concentration of SWCNT based on several experimental observations. To produce UHMWPE filament from a viscous gel, the gel viscosity is an important factor. The gel viscosity varies based on the nanotube concentrations and the viscosity should be such that it could flow easily through the outlet die during the extrusion process. The speed of the rotor was kept low to avoid excessive applied shear. When the concentration of SWCNTs was high (above 2.0 wt.%), flow viscosity increased and continuous production of filament was very difficult without applying excessive shear force by the turning rotor at higher speed. As a consequence of high shear force, during the extrusion process, polymer chains started to break and restricted continuous filament production. On the other hand, a low concentration (lower than 1 wt.%) was less effective on the property improvements. Such phenomena have also been mentioned in our previous paper (Ref 2). In addition, past research (Ref 15, 22) of reinforcement of nanoparticles/nanotubes in thermoplastic polymers also suggests that concentrations of CNTs usually vary between 1 and 2 wt.%, especially with the melt extrusion method.

### 2.2 Strain Hardening of Filaments

Filament samples were strain hardened through a series of loading-unloading cycles using a Zwick-Roell material testing machine. The yield point ($\sigma_y$) for both neat and nanocomposite systems was first determined from uniaxial tension tests of the produced filaments using the standardized method specified in the ASTM D3379-75 report. Tests were run under displacement control at a constant crosshead speed of 2 mm/min using a 20 N load cell. About ten individual filaments were tested in each category. Once the yield point for a particular system is known, samples were first loaded up to a point slightly beyond the yield point ($\sigma = \sigma_y + \Delta\sigma$) and then unloaded to zero load level. This completed the first loop. In the next step, samples were loaded again to a higher point ($\sigma_{new} = \sigma_{old} + \Delta\sigma$) and then unloaded to zero load. This formed the second loop. Such a loading and unloading process was continued until the tested filament was failed. A set of true stress and strain hysteresis curves for each type of filaments was generated in this manner.

## 3. Shear Lag Model

It is known that when the particles are fiber-like such as carbon nanotubes and aligned in a particular direction, the shear lag

model can be used (Ref 17, 22, 23). The governing differential equation for stress distribution in the fiber can be written as

$$\frac{d^2\sigma_f}{dx^2} = \frac{n^2}{r^2}(\sigma_f - E_f\varepsilon_1) \quad \text{(Eq 1)}$$

where $x$ is the distance from the midpoint of the tube, $r$ is the radius of the fiber/tube, $\varepsilon_1$ is the composite strain, and $n$ is a dimensionless constant given by

$$n = \left[\frac{2E_m}{E_f(1+\nu_m)\ln(1/c)}\right]^{1/2} \quad \text{(Eq 2)}$$

m and f subscripts are for matrix polymer and inclusion, respectively, and, $c$ is the volume fraction of the reinforcement. The above second-order differential equation can be solved by applying the boundary conditions of $\sigma_f = 0$ at $x = \pm L \ldots$, where $L$ is the fiber half-length, and defining fiber aspect ratio $L/r = s$, one can derive

$$\sigma_f = E_f\varepsilon_1\left[1 - \cosh\left(\frac{nx}{r}\right)\operatorname{sec} h(ns)\right] \quad \text{(Eq 3)}$$

The stress of the composite can now be determined from the rule of mixture as

$$\sigma_c = (1-c)\sigma_{matrix} + c\sigma_f \quad \text{(Eq 4)}$$

with the average matrix stress ( $\sigma_{matrix}$) taken as its Young's modulus times, the composite strain and the average fiber stress ($\sigma_f$) obtained by integrating Eq 3 over the length of the fiber. This leads to

$$\sigma_f = f\varepsilon_1 E_f\left[1 - \frac{\tanh(ns)}{ns}\right] + (1-f)E_m \quad \text{(Eq 5)}$$

### 3.1 Upper and Lower Bounds of Modulus

Theoretic bounds of composite materials have been extensively treated by micromechanical theories. From the principle of minimum complementary energy, equations of equilibrium, and satisfying the specified boundary conditions on a uniaxial test specimen with normal stresses at the end (Ref 24), one can show that

$$\frac{1}{E_c^-} \le \frac{1-C}{E_p} + \frac{C}{E_i} \quad \text{(Eq 6)}$$

where $E_c^-$ is the lower bound of the longitudinal modulus and p and i subscripts are for polymer and inclusion, respectively. $C$ is the volume fraction of inclusion.

To determine the upper bound, one can begin by subjecting the basic uniaxial test specimen to an elongation, estimate associate strain energy $U^*$, utilize inequality that actual strain energy $U \le U^*$, and come up with

$$E_c^+ \le \frac{1-\nu_i-4\nu_i\nu+2\nu^2}{1-\nu_i-2\nu_i^2}E_iC + \frac{1-\nu_p-4\nu_p\nu+2\nu^2}{1-\nu_p-2\nu_p^2}E_p(1-C) \quad \text{(Eq 7)}$$

where $E_c^+$ the upper bound of the longitudinal modulus $\nu$ is the Poisson's ratio.

## 4. MD Simulations

Molecular models of polymer nanocomposites were developed by infusing a SWCNT in the linear PE matrixes shown in Fig. 1(b). The radius and length of SWNT were chosen as 11 and 30 Å, respectively. In the nanocomposite, the PE matrix was represented by united atom (UA)-$CH_2$- units. The initial structure was constructed by positioning the SWCNT at the center of the unit cell and by randomly generating PE chain(s) on a tetrahedron lattice surrounding SWCNT. The number of polymer chain, number of mers (-$CH_2$-), and molecular weight were 1, 1022, and 14328 g/mol, respectively. The same chain structures were used to describe the polymer in the neat system. The molecular model was generated in a 64 $nm^3$ cubic unit cell.

Once the initial molecular structures for the neat PE and SWNT-PE nanocomposites were developed, corresponding molecular mechanics force fields were then defined. In the simulation, all PE chains are described by appropriate potential functions that include 2-body, 3-body, and 4-body potentials between -$CH_2$-UA units (Ref 25). Specifically, the bond energy

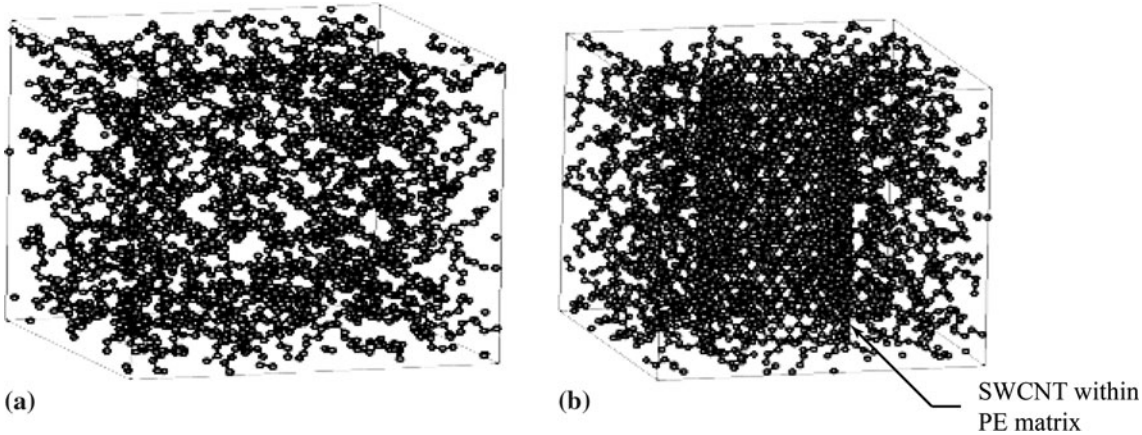


**Fig. 1** (a) Polymer matrix $(-CH_2)_n$ unit cell (64 $nm^3$), (b) nanocomposite model, 3D view

between -$CH_2$- units of the PE chain is determined by the harmonic function:

$$U_{\text{bond}}(r) = \frac{1}{2}k_{\text{r}}[r - r_0]^2 \quad \text{(Eq 8)}$$

where $U_{\text{bond}}(r)$ is the bond potential energy, $r$ is the angle between two bonds, $k_{\text{r}}$ = 700 kcal/mol, and $r_0$ = 1.53 Å. The angle-bending energy or the 3-body term is modeled with a harmonic-cosine valence-angle potential of the form,

$$U_{\text{angle}}(\theta) = \frac{1}{2}k_{\theta}[\cos(\theta) - \cos(\theta_0)]^2 \quad \text{(Eq 9)}$$

where $U_{\text{angle}}(\theta)$ is the angle-bending potential energy, θ is the angle between two bonds, $k_\theta$ = 112.5 kcal/mol, and $\theta_0$ = 109.471. The functional form of the 4-body term or the dihedral potential energy is prescribed by

$$U_{\text{dihedral}}(\varphi) = k\varphi[1 + \cos(m\varphi)] \quad \text{(Eq 10)}$$

Here, $U_{\text{dihedral}}(\phi)$ is the dihedral energy, ϕ is the dihedral angle around the $CH_2$-$CH_2$ bond, $k_\phi$ = 1.0 kcal/mol, and $m$ = 3.0.

The non-bonded van der Waals (VDW) interactions within or between PE chains are modeled with the Lennard-Jones (LJ) potential (Ref 26),

$$U_{\text{LJ}}(r) = 4u\left[\left(\frac{a}{r}\right)^{12} - \left(\frac{a}{r}\right)^{6}\right] \quad \text{(Eq 11)}$$

where $U_{\text{LJ}}(r)$ is the potential energy between a pair of atoms, $r$ is the separation distance between them, $u$ is the potential well depth, and $a$ is the VDW separation distance. For the interaction between the -$CH_2$- units, the potential was parameterized with $u$ = 0.113266 kcal/mol and $a$ = 4.28 Å.

The SWNT particle was modeled as a non-deformable solid inclusion by "freezing" all C atoms during MD simulation. The non-bonded interactions between PE and frozen buckyballs were modeled and evaluated by the LJ potential, and the corresponding parameters for perfect interaction are $u$ = 0.107290 kcal/mol and $a$ = 3.825 Å.

All simulations were carried out at a temperature of 300 K with 0.5 fs time steps. The elastic properties of neat polymer and nanocomposites were evaluated by performing simulations in two major steps. In the first step, the equilibrium state of the molecular model was obtained. In the next step, the model was subjected to different strain fields and then reequilibrated. From the MD point of view, attainment of such an equilibrium state requires fulfillment of two major criteria, i.e., achieving an energy-stabilized state at a prescribed temperature and obtaining the minimum initial stress state for the unit cell. In the current study, an energy-stabilized state was achieved by consecutively subjecting the initial model to canonical (constant-NVT) and microcanonical (constant-NVE) ensembles for 50,000 and 10,000 steps, respectively. Next, the initial stresses were minimized by adjusting the size of the unit cell using isothermal-isobaric (constant-NPT) ensembles for several thousand steps and subsequently equilibrating the system by NVE for 10,000 steps. At the end of these steps, the molecular model was considered to be relaxed at 300 K and with minimum initial stresses.

For each model at the equilibrated state, a uniform strain field (1%) along the $z$ direction (longitudinal direction of the nanotube) was applied by proportionately scaling the size of the unit cell and the atomic positions of PE chain and SWCNT. All systems were then run for 30,000 steps using NVE. The last 10,000 steps were the "production run" and the first 20,000 steps were the equilibration run. For every 10th time step during the production run, the volume averaged virial stresses were obtained as follows (Ref 27).

$$\sigma_{ij} = -\frac{1}{V}\sum_{\alpha}\left(M^{\alpha}v_i^{\alpha}v_j^{\alpha} + \frac{1}{2}\sum_{\beta\neq\alpha}F_i^{\alpha\beta}r_j^{\alpha\beta}\right) \quad \text{(Eq 12)}$$

where $V$ is the volume of the unit cell and equal to the sum of the atomic volumes of all the atoms. $v_i^{\alpha}$ is the $i$-component of the velocity of atom α, $v_j^{\alpha}$ is the $j$ component of the velocity of atom α, $F_i^{\alpha\beta}$ is the $i$ component of the force acting between atoms α and β, and $r_j^{\alpha\beta}$ is the $j$ component of separation distance between atoms α and β. Here, the first term is associated with the contribution from kinetic energy due to thermal vibration and the second term is related to change in potential energy due to applied deformation. The negative sign is used to express tensile stress as a positive quantity, as opposed to the sign conventionally used in MD which treats compression as a positive quantity. Each stress component obtained from every 10th time step during the production run was recorded and averaged. These stress components are considered as the corresponding stress components resulting from the applied strain field. The elastic behavior of the molecular systems was described using continuum mechanics. It is assumed that both neat polymer and nanocomposite possess isotropic material symmetry, and a linear elastic stress-strain relation prevails. Under these assumptions, the generalized constitutive relation of the equivalent continuum can be reduced to (Ref 27)

$$[\sigma_{ij}] = [C_{ij}][\varepsilon_{ij}]$$

where $\sigma_{ij}$, $C_{ij}$, and $\varepsilon_{ij}$ are the stress, elastic constant, and strain tensors, respectively.

## 5. Results and Discussions

### 5.1 Experimental

Representative stress-strain diagrams and the data from tensile tests for neat and reinforced polymer filaments are shown in Fig. 2 and Table 1. It was observed that with the infusion of SWCNTs, the ultimate tensile strength and Young's modulus of neat UHMWPE were increased by 120 and 463%, respectively. It was also noticed that yield strength (0.2% offset) was increased by almost 500% with the addition of SWCNTs. Figure 3 shows the representative true stress versus strain hysteresis curves for these two categories of filaments. Elastic properties were evaluated at the last loading cycle just before the failure of the filaments and are presented in Table 2. The strength level shows a gradual increase for all kinds of samples after several hysteresis loops. The increase in strength is clearly higher in nanophased samples compared to the neat, as can be seen in Fig. 3. It is also seen that around 200% strain was possible for both neat and UHMWPE-SWCNT filaments through repeated loading-unloading cycles. At such large strain, both strength and modulus were also higher. For instance, the ultimate tensile strength and modulus of neat UHMWPE samples were found to be nearly 1 and 4 GPa, respectively, which exceed the values obtained from the

monotonic tensile test by a large margin. The magnitudes of the elastic properties were further enhanced with the infusion of SWCNTs. When filaments with SWCNTs were strain hardened, the ultimate tensile strength and modulus were increased to roughly 2 and 14 GPa, respectively, which is 116 and 253% more than those of neat filaments after strain hardening.

The enhanced elastic properties after strain hardening reported here for the SWCNT-reinforced UHMWPE filaments are expected due to the high degree of alignment of both the polymer and the nanotubes. Figure 3(a) shows much improved orientation of the polymer fibrils and Fig. 4(b) represents an array of nanotubes partially aligned within the matrix polymer; both were achieved through the strain hardening cycles. This suggests that molecular rearrangements have taken place during loading and unloading operations, giving rise to the observed stress-strain response. The large increase in strength also suggests exceptionally high interfacial shear strength between the matrix and the nanotubes. We noticed significant polymer wettings around the nanotube, as shown in Fig. 4(c). CNTs can act as strong nucleation agents/sites, where crystalline polymer segregates and forms hard crystal segments. These hard segments attached to the nanotubes can effectively transfer the load to nanotubes. Higher values of strength and modulus seen in strain-hardened UHMWPE-SWCNT filaments are the direct consequences of improved alignment and coating of nanotubes.

Figure 5 shows the spectral distribution of the Raman shift of the UHMWPE-SWCNT filament before and after strain hardening. Raman spectroscopy is an effective technique to provide information regarding the response of the molecules under stress and deformation. It has been widely used to investigate the deformation of fibers at the molecular level, particularly in a monofilament form. Raman spectra of individual filaments were obtained using a T64000 spectrometer with a 514.5 nm line of argon ion laser and a highly sensitive Charged Couple Device. When polymers are deformed, the bonds in the molecules are strained, and some

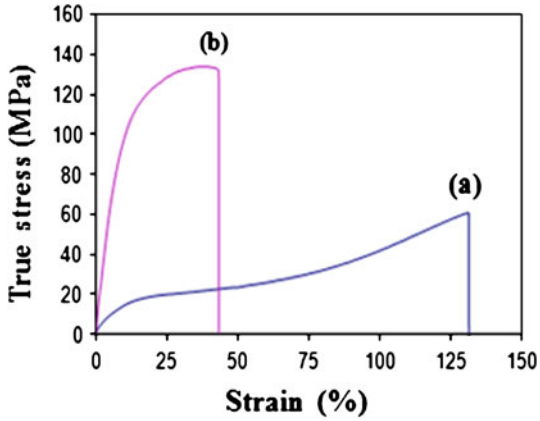


**Fig. 2** Tensile stress-strain curves of (a) neat UHMWPE, (b) UHMWPE-SWCNT

of the frequencies of Raman bands are shifted to lower or higher wave numbers depending on the tension or compression in the molecular bonds. The C-C asymmetric stretching mode (1064 $cm^{-1}$) and symmetric stretching mode (1130 $cm^{-1}$) of PE are observed. The orthorhombic crystalline phase is represented by 1417 $cm^{-1}$ band, whereas 1296 $cm^{-1}$ indicates the $CH_2$ wagging mode for PE (Ref 28-30). The band at 1593 $cm^{-1}$ and 1350 $cm^{-1}$ is the characteristic *G* and *D* band for infused SWCNTs. *D* band arises from the disorder-induced mode $Ag_1$ (Ref 31-34). After strain hardening of UHMWPE-SWCNT samples, *D* and *G* bands shifted to 1358 and 1591 $cm^{-1}$, respectively (Fig. 5b). The positive shift in *D* band suggesting a lateral compression of nanotubes occurred at the defect sites due to the strain hardening. It is also seen that the ***G*** band which represents the tangential C-C bonds in the nanotubes moves to a lower wave number (1591 $cm^{-1}$) after strain hardening. It indicates that the stress has been transferred from the matrix to nanotubes, which tend to stretch the SWCNTs. However, there was no significant change in the intensity ratio ($I_D/I_G$) of *D* and *G* bands before and after strain hardening as can be observed from Fig. 5(a) and (b). This suggested that no structural defect was generated in the SWCNTs due to the loading-unloading cycles.

### 5.2 Theoretic Prediction

A first-order estimation for the theoretic strength of the composites can be made using Eq 3 and 4 of the shear lag model, assuming that the total matrix strain at failure is the composite strain at failure. The matrix (UHMWPE) properties were used from Tables 1 and 2 before and after strain hardening, respectively. The density and Poisson's ratio of UHMWPE were 0.9 $g/cm^3$ and 0.4, respectively. Property values for SWCNT were used from the literature (Ref 35), and the values of Young's modulus, density, and Poisson's ratio of SWCNT were chosen to be 1.5 TPa, 2.6 $g/cm^3$, and 0.28, respectively. The volume fraction of SWCNT was 0.00724. The strength of the UHMWPE-SWCNT composites was found to be in the range of 62 MPa to 2.7 GPa before strain hardening, which was increased to the range of 0.97 to 3.4 GPa after strain hardening. In the context of experimental measurement, the strength levels of the reinforced filaments were 134 MPa and 2.1 GPa before and after strain hardening, respectively. It is therefore seen that the experimental strength of the SWCNT-reinforced UHMWPE after strain hardening is in close agreement with the predicted higher limit of strength. Since, in reality, there is a significant difference between composite failure strain and matrix failure strain for the non-strain-hardened system, the predicted composite strength is therefore not in very close agreement with the experimental results. The Young's modulus of the composites was calculated using Eq 5 and 6. The lower limit of the modulus is the modulus of the matrix; however, the upper limits of the modulus of UHMWPE-SWCNT composites were found to be 10.7 and 14.4 GPa before and after strain hardening, respectively. It was observed that there is a significant difference between the

**Table 1 Tensile test data**

| Type | Exp. strength, MPa | Calc. strength, MPa | Exp. modulus, MPa | Calc. modulus, MPa |
|---|---|---|---|---|
| UHMWPE | 61 ± 6 | NA | 238 ± 17 | NA |
| UHMWPE + SWCNT | 134 ± 9 | 62-2700 | 1340 ± 21 | 10,780 |

predicted upper limit of modulus and the experimental modulus before strain hardening. However, the experimental modulus of UHMWPE-SWCNT composites after strain hardening is very much close to the predicted upper limit.

### 5.3 MD Simulation

The linear elastic stress-strain relation and elastic modulus of neat PE and SWCNT-reinforced nanocomposites obtained from MD simulations are presented in Table 3. To obtain better statistics of the results, the entire simulation procedure was repeated three times with an arbitrary starting configuration of either neat PE or SWCNT-reinforced nanocomposites. The results shown in Table 3 represent the average properties of the simulated structures. The corresponding experimental results are also listed in Table 3. It is important to note that the maximum achievable strain of the simulated samples was 1%.

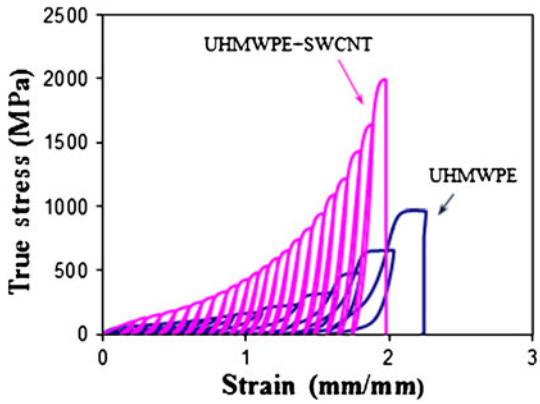


**Fig. 3** Cyclic true stress-strain hysteresis curves for neat and nanophased UHMWPE filament

Therefore, we chose the stress value at 1% strain for comparison.

It is observed in Table 3 that the stress value of simulated neat PE at 1% of strain was 48.6 MPa. The same polymer matrix showed a significant increase (~53%) in stress level due to the reinforcement by SWCNT. Similarly, elastic modulus was increased ~54% (from 4.8 to 7.4 GPa) by the addition of SWCNT. In the context of polymer strengthening by adding SWCNT, our simulation observations agree with the experimental observations qualitatively. However, quantitative analyses of our data show that the results (stress at 1% strain and modulus) obtained before strain hardening were extremely low compared to MD predications; hence, we excluded those from our discussion. However, the experimental results obtained after strain hardening were in agreement, to some extent, both for neat and reinforced polymer samples, as shown in Table 3. MD predictions of stress at 1% strain and modulus were ~30% more than the experimentally measured values of strain-hardened neat UHMWPE samples. However, when PE samples were reinforced and strain hardened, simulation results underpredict both stress (at 1% strain) and modulus by ~45% than experimentally measured values.

The discrepancies between MD observations and the results obtained experimentally after strain hardening can be explained on the basis of idealization of the model used in MD simulation. The structure used in MD was generated by placing the PE chain randomly within the tetrahedron. Therefore, the simulated structure was more amorphous rather than crystalline. However, in practice, pure amorphous PE is not available and a considerable percentage of crystallinity exists in UHMWPE structure. Moreover, this crystallinity increased due to the infusion of SWCNT. In addition, strain hardening also has some direct influence on the material properties. Strain hardening causes partial alignment of the polymer chains,

**Table 2 Test data after strain hardening**

| Type | Exp. strength, GPa | Calc. strength, GPa | Exp. modulus, GPa | Calc. modulus, GPa |
|---|---|---|---|---|
| UHMWPE | 0.97 ± 0.03 | NA | 3.9 ± 0.2 | NA |
| UHMWPE + SWCNT | 2.1 ± 0.07 | 0.97-3.4 | 13.8 ± 0.3 | 14.4 |

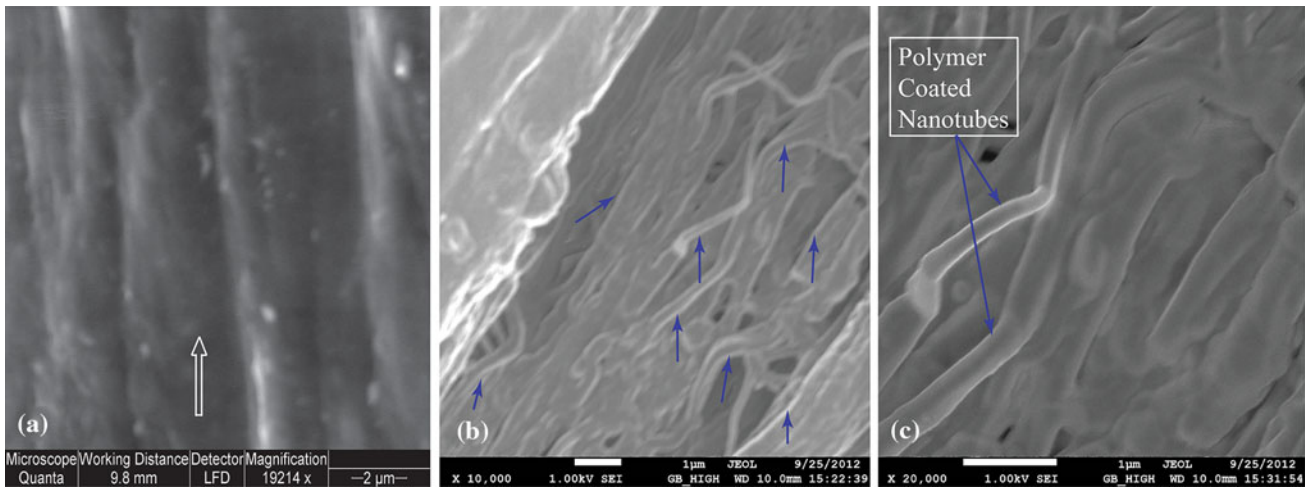


**Fig. 4** SEM micrographs of (a) oriented UHMWPE fibrils, (b) partially aligned array of nanotubes, and (c) nanotube coated with thick polymer

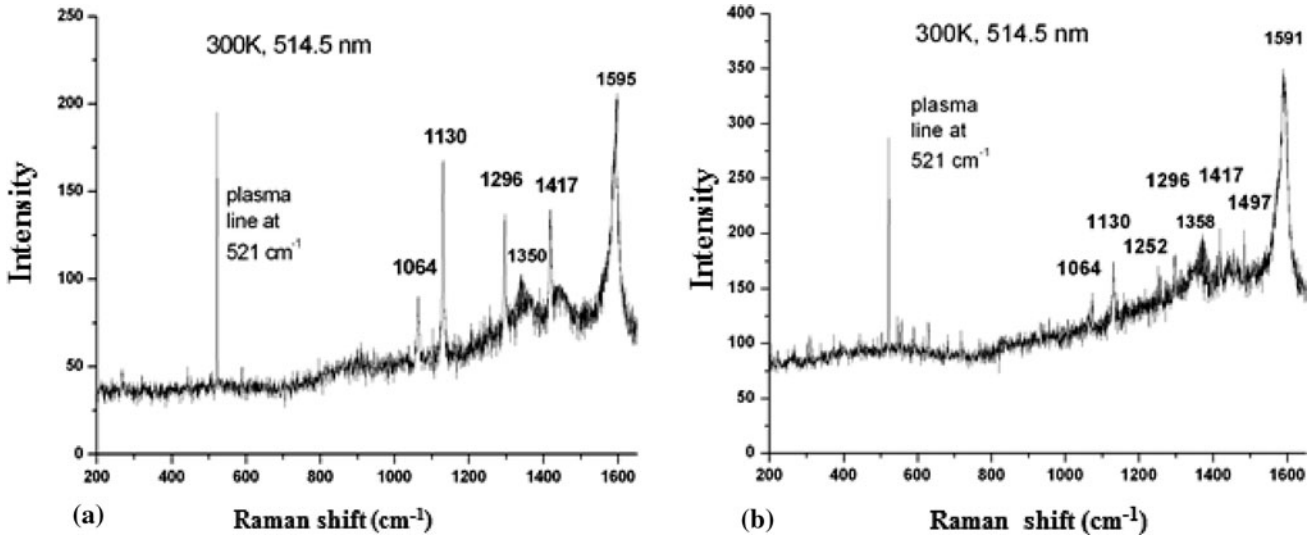


**Fig. 5** Raman spectrums of (a) UHMWPE-SWCNT, (b) UHMWPE-SWCNT after strain hardening

**Table 3 Simulated and experimental values of strength and modulus**

| | UHMWPE matrix | | UHMWPE-SWCNT | |
|---|---|---|---|---|
| | MD simulation | Experimental (after strain hardening) | MD simulation | Experimental (after strain hardening) |
| Stress at 1% strain, $\sigma_{zz}$, MPa | 48.6 | $37.1 \pm 1.8$ | 74.2 | $134.3 \pm 5.4$ |
| Elastic modulus, $C_{33}$, GPa | 4.8 | $3.7 \pm 0.17$ | 7.4 | $13.8 \pm 0.27$ |

which ultimately contribute to enhanced strength. As pointed out in the previous section, experimental observations showed significant polymer wettings around nanotubes, which result in a high interfacial strength and enhanced load transfer between the matrix and nanotubes. However, in MD simulation, only a non-bonded Van der waals interaction was considered between the nanotube and the surrounding polymer atoms.

## 6. Summary

1. A methodology to reinforce UHMWPE with carbon nanotubes is presented. The process involves solution spinning followed by melt extrusion and can be employed for any PE-based polymers.
2. Although the concentration of nanotubes was only at 2.0 wt.%, the improvement in mechanical properties was significant. Ultimate tensile strength and modulus were increased by 120 and 463%, respectively.
3. A procedure for strain hardening of extruded fibers is also introduced to investigate fiber properties at maximum possible strain. It has been observed that after strain hardening, strength and modulus increased by almost one order of magnitude. With the SWCNT reinforcement, these improvements are even higher. Strength of neat UHMWPE increases from 61 MPa to 2.1 GPa and modulus increased from 238 MPa to 13.8 GPa.
4. It was seen that after strain hardening of the SWCNT-reinforced UHMWPE, the experimental strength is in close agreement with that of the predicted higher limit of strength calculated using the shear lag model.
5. It was observed that there is a significant difference between the predicted upper limit of modulus and the experimental modulus before strain hardening. However, the experimental modulus of UHMWPE-SWCNT composites after strain hardening is very much close to the predicted upper limit.
6. A molecular simulation study was conducted. It was observed that the predicted values were only comparable with those obtained after strain hardening. In the case of UHMWPE-SWCNT, the predicted stress (at 1% strain) and modulus were ~45% less than those of strain-hardened nanocomposites. The discrepancy is believed to be due to many possible reasons including the consideration of amorphous polymer in the simulated structure.


### Acknowledgments

The authors would like to acknowledge support from the National Science Foundation (NSF) for this work through Grant No. HRD-976871. The authors would also like to thank Dr. Efthymios Liarokapis and Dr. Mahmoud Madani for their assistance in Raman Spectroscopy and SEM analysis.


### References


1. M.R. Khan, H. Mahfuz, Th. Leventouri, V.K. Rangari, and A. Kyriacou, Enhancing Toughness of Low-Density Polyethylene Filaments Through Infusion of Multiwalled Carbon Nanotubes and Ultrahigh Molecular Weight Polyethylene, *Polym. Eng. Sci.*, 2011, **51**(4), p 654–662

2. H. Mahfuz, M.R. Khan, Th. Leventouri, and E. Liarokapis, Investigation of MWCNT Reinforcement on the Strain Hardening Behavior of Ultra high Molecular Weight Polyethylene, *J. Nanotech.*, Article ID 637395, 2011
3. M.R. Khan, H. Mahfuz, and Th Leventouri, Effect of Strain Hardening on the Elastic Properties and Normalized Velocity of Hybrid UHMWPE-Nylon 6-SWCNT Nanocomposites Fiber, *J. Mater. Res.*, 2012, **27**(20), p 2657–2667
4. H. Mahfuz, M. Hasan, V. Dhanak, G. Beamson, J. Stewart, V. Rangari, X. Wei, V. Khabashesku, and S. Jeelani, Reinforcement of Nylon 6 with Functionalized Silica Nanoparticles for Enhanced Tensile Strength and Modulus, *Nanotechnology*, 2008, **19**(44), p 445702
5. J.P. Salvent, G.A.D. Briggs, J.M. Bonard, R.R. Bacsa, A.J. Kulik, T. Stockli, N.A. Burnham, and L. Forro, Elastic and Shear Moduli of Single-Walled Carbon Nanotube Ropes, *Phys. Rev. Lett.*, 1999, **82**(5), p 944–947
6. F. Li, H.M. Cheng, S. Bai, G. Su, and M.S. Dresselhaus, Tensile Strength of Single-Walled Carbon Nanotubes Directly Measured from Their Macroscopic Ropes, *Appl. Phys. Lett.*, 2000, **77**(20), p 3161–3163
7. C. Li and T.W. Chou, Elastic Moduli of Multi-Walled Carbon Nanotubes and the Effect of Van Der Waals Forces, *Compos. Sci. Technol.*, 2003, **63**, p 1517–1524
8. L. Jin, C. Bower, and O. Zhou, Alignment of Carbon Nanotubes in a Polymer Matrix by Mechanical Stretching, *Appl. Phys. Lett.*, 1998, **73**, p 1197–1199
9. C.A. Cooper, D. Ravich, D. Lips, J. Mayer, and H.D. Wagner, Distribution and Alignment of Carbon Nanotubes and Nanofibrils in a Polymer Matrix, *Compos. Sci. Technol.*, 2002, **62**, p 1105–1112
10. E.T. Thostenson and T.W. Chou, Aligned Multi-Walled Carbon Nanotube-Reinforced Composites: Processing and Mechanical Characterization, *J. Phys. D*, 2002, **35**(16), p 77–80
11. H.R. Brown, Studies of Orientation and Structure of Crazed Matter in Polystyrene I, Optical Measurements, *J. Polym. Sci. Polym. Phys. Ed.*, 1979, **17**(8), p 1417–1430
12. A.J. Kinloch and R.J. Young, *Fracture Behaviour of Polymers*, Elsevier, London, 1988
13. C. Zhao, G. Hu, and R. Justice, Synthesis and Characterization of Multi-Walled Carbon Nanotubes Reinforced Polyamide 6 via In Situ Polymerization, *Polymer*, 2005, **46**(14), p 5125–5132
14. S. Ruan, P. Gao, and T.X. Yu, Ultra-Strong Gel-Spun UHMWPE Fibers Reinforced Using Multiwalled Carbon Nanotubes, *Polymer*, 2006, **47**(5), p 1604–1611
15. H. Mahfuz, M.M. Hassan, V.K. Rangari, and S. Jeelani, Reinforcement of Nylon 6 Filaments with $SiO_2$ Nanoparticles and Comparison of Young's Modulus with Theoretical Bounds, *Macromol. Mater. Eng.*, 2007, **292**, p 437–444
16. X.L. Gao and K. Li, A Shear-Lag Model for Carbon Nanotube-Reinforced Polymer Composites, *Int. J. Solid. Struct.*, 2005, **42**, p 1649–1667
17. H.L. Cox, The Elasticity and Strength of Paper and Other Fibrous Materials, *Brit. J. Appl. Phys.*, 1952, **3**, p 72–79
18. A. Al-Ostaz, G. Pal, P.R. Mantena, and A. Cheng, Molecular Dynamics Simulation of SWCNT-Polymer Nanocomposite and Its Constituents, *J. Mater. Sci.*, 2008, **43**, p 164–173
19. S.J.V. Frankland, A. Caglar, D.W. Brenner, D. Wand, and M. Griebel, Molecular Simulation of the Influence of Chemical Cross-Links on the Shear Strength of Carbon Nanotube-Polymer Interfaces, *J. Phys. Chem. B.*, 2002, **10**(6), p 3046
20. S.J.V. Frankland, V.M. Harik, G.M. Odegard, D.W. Brenner, and T.S. Gates, The Stress-Strain Behavior of Polymer-Nanotube Composites from Molecular Dynamics Simulation, *Compos. Sci. Technol.*, 2003, **63**, p 1655
21. M. Griebel and J. Hamaekers, Molecular Dynamics Simulations of the Elastic Moduli of Polymer-Carbon Nanotube Composites, *Comput. Meth. Appl. Mech. Eng.*, 2004, **193**, p 1773
22. H. Mahfuz, A. Adnan, V. Rangari, M.M. Hasan, S. Jeelani, W.J. Wright, and S.J. Deteresa, Enhancement of Strength and Stiffness of Nylon 6 Filaments Through Carbon Nanotubes Reinforcement, *Appl. Phys. Lett.*, 2006, **8**(8), p 083119
23. D. Hull and T.W. Clyne, *An Introduction to Composite Materials*, Cambridge University Press, Cambridge, 1996
24. R. Jones, *Mechanics of Composites Materials*, 2nd ed., Hemisphere Publishing Corporation, New York, 1998
25. W. Smith, T.R. Forester, DLPOLY-2.19 manual, http://cms.kist.re.kr/code/DL_POLY/manual/MANUAL_2.pdf. Accessed Dec 2010
26. M.P. Allen and D.J. Tildesley, *Computer Simulation of Liquids*, Oxford university press, Oxford, 2001
27. A. Ashfaq, C.T. Sun, and H. Mahfuz, A Molecular Dynamics Simulation Study to Investigate the Effect of Filler Size on Elastic Properties of Polymer Nanocomposites, *Compos. Sci. Technol.*, 2007, **67**, p 348–356
28. W.F. Wong and R.J. Young, Analysis of the Deformation of Gel-Spun Polyethylene Fibres Using Raman Spectroscopy, *J. Mater. Sci.*, 1994, **29**, p 510–519
29. B.J. Kip, M.C.P. Van Eijk, and R.J. Meier, Molecular Deformation of High-Modulus Polyethylene Fibers Studied by Micro-Raman Spectroscopy, *J. Polym. Sci. B*, 1991, **29**, p 99–108
30. A. Cooper, R.J. Young, and M. Halsall, Investigation into the Deformation of Carbon Nanotubes and Their Composites Through the Use of Raman Spectroscopy, *Compos. A*, 2001, **32**, p 401–411
31. G. Socrates, *Infrared and Raman Characteristic Group Frequencies Tables and Charts*, 3rd ed., Wiley, New York, 2001
32. R.J. Nemanich and S.A. Solin, First- and Second-Order Raman Scattering from Finite-Size Crystals of Graphite, *Phys. Rev. B*, 1979, **20**, p 392
33. M.G. Donato, G. Messina, and S. Santangelo, Aid of Raman Spectroscopy in Diagnostics of MWCNT Synthesised by Fe-Catalysed CVD, *J. Phys. Conf.*, 2007, **61**, p 931–935
34. M.S. Dresselhous, M.A. Pimenta, and P.C. Eklund, *Raman Scattering in Material Science*, Springer, Berlin, 2000
35. Y. Gogotsi, *Nanomaterials Hand Book*, Taylor and Francis Group, Boca Raton, FL, 2006